



Investigation of the effects of machining parameters on cutting conditions during orthogonal turning of austenite stainless steel

Gábor Kónya^{1*}, János Takács², István Miskolczi¹, Zsolt F. Kovács¹

¹ GAMF Faculty of Engineering and Computer Science, Department of Innovative Vehicles and Materials, John von Neumann University, Izsáki út 10., H-6000 Kecskemét, Hungary; konya.gabor@nje.hu (GK); miskolczi.istvan@nje.hu (IM); kovacs.zsolt@nje.hu (ZFK)

² Faculty of Transportation Engineering and Vehicle Engineering, Department of Automotive Technologies, Budapest University of Technology and Economics, Műgyetem rkp. 3., H-1111 Budapest, Hungary, ORCID 0000-0002-3849-5753, e-mail: takacs.janos@kjk.bme.hu

*Correspondence: konya.gabor@nje.hu

Article history

Received 18.09.2023

Accepted 08.01.2024

Available online 29.02.2024

Keywords

Taguchi orthogonal turning, cutting forces, cutting temperature, chip morphology, tool wear.

Abstract

The 1.4306 austenite stainless steel has been prominently utilized as a material in the automotive and aerospace industry. Considerable interest has been garnered in the machinability of stainless steel owing to its high strength and poor thermal conductivity. The aim of this study is to ascertain the influential cutting parameters, specifically the cutting speed and feed rate, on cutting forces, cutting temperature, and chip evaluation. Thus, austenite stainless steel was subjected to free-cutting using a carbide recessing tool under dry conditions. The principle of measuring cutting temperature, a complex procedure due to varying thermal homogeneity, was elucidated. For the turning experiments in question, the standard Taguchi orthogonal array L9 (3²), featuring two factors and three levels, was employed. The experimental results were analyzed using MiniTab 17 software. The findings reveal a substantial effect of feed rate on cutting force, cutting temperature, and chip evaluation. The highest cutting force and cutting temperature were observed at a feed rate of 0.15 mm/rev. Conversely, the cutting force was minimized at a cutting speed of 100 m/min, indicating potential for increasing the cutting speed. The augmentation of feed rate led to chip compression and discoloration, attributed to elevated cutting force and a larger chip cross-section that efficiently dissipates heat from the cutting zone.

DOI: 10.30657/pea.2024.30.8

1. Introduction

Stainless steels are extensively utilized in diverse industries, including automotive and aerospace (Szcotkarz et al., 2021), medical equipment (Acayaba and de Escalona, 2015), food industry (Kulkarni et al., 2014) and nuclear applications (Bharasi et al., 2019) owing to their outstanding mechanical characteristics, elevated corrosion resistance, durability, and aesthetic appeal. These materials are classified as a difficult-to-machine materials due to their high toughness, low thermal conductivity, and pronounced work hardening. Consequently, these properties contribute to rapid tool wear during machining operations. Researchers are currently engaged in exploring and analyzing the machinability aspects of various types of stainless steels. This investigative focus encompasses different stainless steel variants such as 304 (Kulkarni et al., 2014),

316L (Saketi et al., 2016), and duplex stainless steel (Krolczyk et al., 2015). Understanding and improving the machinability of stainless steels is a crucial goal for researchers. By exploring the complexities of machining these materials, such as optimizing cutting parameters, tool materials, and cooling strategies, their objective is to reduce tool wear and increase productivity.

Smith stated the machinability is the sum of all properties of the workpiece material that affect the cutting process and the relative ease with which a satisfactory product can be produced by the machining process (Smith, 1989). The machinability of a material is closely tied to the lifespan of the cutting tool. Tool life is the duration, measured in minutes, during which a cutting edge affected by the cutting process, retains its cutting capabilities until the need for sharpening arises. The cutting edge remains functional until a specific level of wear



takes place (Tschätsch and Reichelt, 2009). Tool life and machinability in the turning process is determined by numerous factors, such as tool data, cutting data, the cooling-lubricating or heating methods, the microstructure, and the mechanical and physical properties of machined the workpiece. These factors are illustrated in the Ishikawa diagram in Fig. 1. The rigidity of the lathe significantly impacts tool life as a result of vibration. When a lathe lacks adequate rigidity, it tends to experience vibrations during machining processes. These vibrations have detrimental effects on the efficiency and lifespan of cutting tools. Excessive vibration contributes to heightened tool wear, decreased cutting accuracy, and diminished surface finish quality on the workpiece. Moreover, it can create fluctuations in cutting forces, intensifying tool deterioration and potentially causing premature tool failure (Gökkaya and Halbant, 2007).

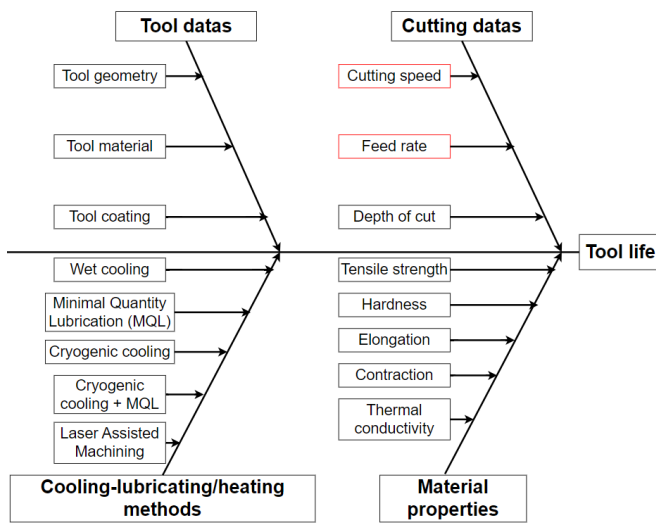


Fig. 1. Ishikawa diagram of the factors influencing tool life

The characteristics of cutting tool, such as tool geometry, tool material composition, and coatings have a huge impact on tool life and applicable process parameters, through which productivity is also greatly affected. For the productive machining of these materials, ceramic, PCBN, and carbide tools with various coatings, such as ZrO₂, SiC, TiC, TiCN, and TiAlN, are commonly used (Radek, 2023).

Tool life is also influenced by the parameters of the process, such as cutting speed, depth of cut, and feed rate (Kun et al., 2019; Sonawane et al., 2021). Kun et al, when milling difficult-to-machine nickel-base superalloys with GTD-111 grades, found that these materials benefit from lower cutting speeds, higher feed rates and more robust tool geometries. The longest tool life was achieved at a cutting speed of 10 m/min and a feed per tooth of 0.03 mm/tooth (Kun et al., 2019). Sonawane et al investigated the effects of cutting speed, feed rate and depth of cut on surface roughness, vibration and tool wear during the turning of Incoloy 600. The results show that feed rate has the largest effect on surface roughness, followed by cutting speed, and depth of cut has no effect on surface roughness. The vibration increased the most with increasing depth of cut, followed by feed rate, in which case it is observed that above a certain parameter, the vibration does not increase

significantly. However, as the cutting speed was increased, the vibration decreased, but above a certain parameter, the decrease was smaller. The most common tool failure was due to fracture, which was attributed to high work hardening (Sonawane et al., 2021). In addition, the optimization of technological parameters nowadays includes the quality of the machined surface, material removal performance, and energy consumption, keeping sustainability in consideration (Móricz and Viharos, 2022; Kovács et al., 2022). Krolczyk et al. have turned 1.4462 duplex stainless steel using MM 2025 and CTC 1135 inserts in dry and emulsion cooling under different process setting. The result was that dry machining achieved a 65 % longer life than emulsion cooling. The effects of cutting speed and feed rate on tool life were investigated and it was found that, in principle, tool life increases at low cutting speeds, but at higher cutting speeds of 0.2 mm/rev feed rate, almost the same tool life was achieved as at low values (Krolczyk et al., 2015). In a study conducted by Kulkarni et al, the focus was on examining how variations in cutting speed and feed rate impact the cutting force and temperature in the process of turning AISI 304 stainless steel. The study's results demonstrated that as cutting speeds increased, there was a decrease in cutting force, contrasting with the consistent rise in cutting force associated with higher feed rates. Moreover, there was a clear connection observed between increased cutting speeds or feed rates and an escalation in cutting temperature (Kulkarni et al., 2014).

The choice of cooling-lubricating methods is a significant factor in tool life (Buranská et al., 2019). Stainless steels are machined using several cooling and heating methods, the most common of which are wet, Minimum Quantity Lubrication (MQL), cryogenic cooling with liquid carbon dioxide or nitrogen, a combination of cryogenic and MQL, and Laser Assisted Machining (LAM) (Leksycki et al., 2023; Venkatesan, 2017; Kónya and Kovács, 2023). Leksycki et al. conducted a comprehensive investigation focusing on the ramifications of employing different cooling methods, namely dry, emulsion, and flood cooling, during the turning process of Ti6Al4V alloy. Their study aimed to analyze and compare how these cooling techniques affect various crucial factors such as chip formation, cutting force dynamics, and the extent of tool wear in the machining of this specific alloy. The study revealed that the least amount of wear was observed with MQL cooling, followed by flood cooling, while the highest wear occurred with dry machining. (Leksycki et al, 2023). Venkatesan turned Inconel 718 in a conventional and laser-assisted environment using a carbide cutting insert. The results showed that in laser-assisted turning, the cutting force applied was halved, surface roughness was almost halved and tool life increased by 60%. This was due to the preheating of the machined surface, which largely prevented work hardening during machining. The effect is also noticeable on the resulting chips, as the serration due to the high shear stress is greatly reduced (Venkatesan, 2017). Kónya and Kovács milled a GTD-111 Ni-based superalloy using a carbide tool with flood cooling and cryogenic cooling with liquid carbon dioxide (LCO₂). They did not observe a large difference in cutting force, but tool wear and pitting were significant with liquid carbon dioxide cooling, and

surface roughness was also impaired. The only improvement was in chip breakage as the material has become brittle, but overall lubrication is more important than cooling in the machining of these difficult-to-machine materials (Kónya and Kovács, 2023).

The material properties, particularly hardness, have a significant impact on the tool life during turning. Hardness is closely related to the material's strength, and it affects the cutting force and temperature. Higher hardness values result in increased cutting forces and temperatures, which increase the mechanical and thermophysical load on the tool edge. The heat generated during the cutting process can cause thermal damage to the tool edge, leading to premature tool failure. This effect is even more significant for these materials because the heat cannot escape as efficiently in the separated chip due to poor thermal conductivity (Kónya et al., 2022). Hard phases, such as carbides in the workpiece can also increase abrasive wear on the cutting tool. Furthermore, the presence of some alloy materials, such as Cr and Ni, in the workpiece can cause self-hardening during machining. When the allowance is removed through successive cuts, the hardness of the already machined upper layers increases, leading to further tool wear (Sipos, 2018). Another wear phenomenon is chemical wear due to high cutting temperatures. Chemical wear occurs when the tool reacts with the workpiece material, such as in the case of high temperature oxidation. These wear mechanisms are more significant for hard-to-cut materials, such as Ni- and Ti-based superalloys and stainless steels (Gerth et al., 2014; Ezugwu and Wang, 1997).

The objective of this paper is to explore and analyze the impacts of two key machining parameters, namely cutting speed and feed rate, which are highlighted in red within the Ishikawa diagram on the resulting cutting forces and temperatures in the context of orthogonal turning. This turning process has been chosen because in this case the separated chips do not cover the cutting zone, thus the thermal camera is able to see the tool edge accurately, giving an accurate temperature value.

2. Methodology

2.1. Experimental environment

The schematic diagram of orthogonal turning with operating forces and the experimental setup is depicted in Fig. 2. The thermal camera is assembled so that its optical axis coincides with the extension of the cutting edge, which is important to ensure that the exact cutting temperature can be measured. A holder is made to hold the thermal camera, which can be adjusted to face perpendicular to the machining plane by holding it in the tailstock.

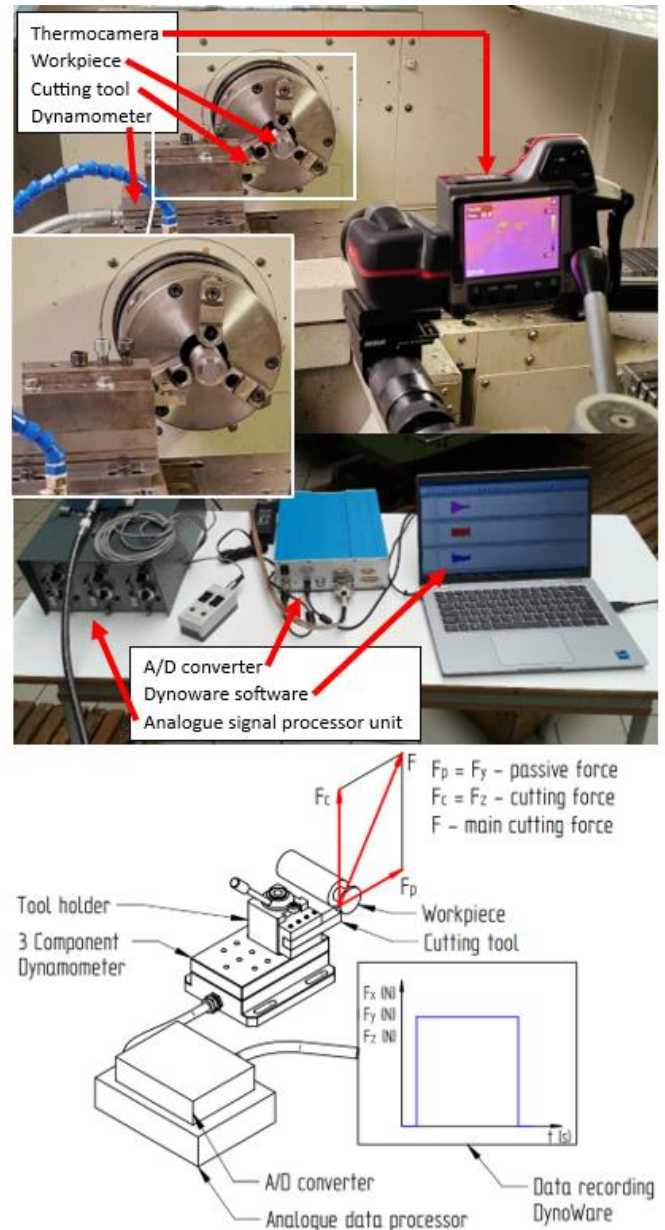


Fig. 2. The principle of force measurement for orthogonal turning

The cutting experiment was conducted on a CNC machine, model NCT BNC-446, ensuring a constant cutting speed throughout the machining process. The KISTLER 9257B type 3 component dynamometer was utilized to measure the cutting forces. To capture the analogue data, sampling was performed at different speeds. The sampling frequency was set so that a signal was recorded for every 3 degrees of workpiece rotation, which is not constant during orthogonal turning because as the diameter decreases, the spindle speed increases. Consequently, the sampling frequency was set to the lowest spindle speed, guaranteeing a sampling interval of every 3 degrees of workpiece rotation at all speeds. This is important because it ensures that for each cutting speed value, a signal is measured at least every 3 degrees, making the results comparable. This was determined using Eq. 1., the calculated and rounded values as a function of applied cutting speed are shown in

Table 1. To process and record the output data, an A/D converter was employed, and the Dynoware software was utilized.

$$f = \frac{n \cdot 120}{60} \text{ (Hz)} \quad (1)$$

Table 1. The calculated and applied sampling (s.) frequency as a function of cutting speed

Cutting speed, (m/min)	Calculated s. freq., (Hz)	Applied s. freq., (Hz)
60	1273.885	1274
80	1698.514	1699
100	2123.142	2124

In the realm of determining cutting force, the conventional approaches often involve calculations based on a singular static force, overlooking the dynamic fluctuations that occur during the cutting process as illustrated in Fig. 3. It can be observed that there is also a minimal fluctuating in the force signal at the start of machining, due to the fact that the insert was not supported on both sides by the workpiece, so the tool was oscillating. At the end of the cutting operation, however, the degree of deflection is even greater in the force signal, which is the result of the tool being stopped while still in the machining, and while the speed and feed rate are decreasing, the tool is working under unfavorable machining conditions. This condition is capable of subjecting the tool to greater stresses than longer periods of machining in a single path.

Recognizing the significance of capturing the dynamic nature of cutting force, it becomes imperative to measure it comprehensively over time. To achieve this, a modern piezoelectric dynamometer with three components was utilized. This dynamometer cell can measure the F_x , F_y , and F_z constituents of the cutting force. By obtaining the values of these force components over machining time, it becomes possible to express and plot the main cutting force in relation to machining time, as described by Eq. (2).

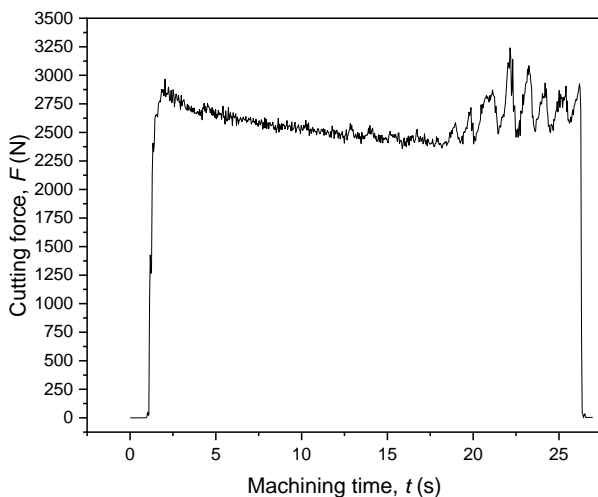


Fig. 3. Main cutting force as a function of machining time in case of 0.05 mm/rev. feed rate and 60 m/min cutting speed

$$F(t) = \sqrt{F_c^2 + F_f^2 + F_p^2} \text{ (N)} \quad (2)$$

For the orthogonal turning, a PVD TiALN-TiN double coated TDC TT9080 (TaeguTec, 2023a) type double ended insert with lead angle and chip breaker was used in a TTER 3232-4T25 tool holder (TaeguTec, 2023b). This blade is specifically recommended by the manufacturer for cutting difficult-to-machine materials at medium feed rates. The point of the 4 mm insert is that this way the two tips are not involved in the machining ($R_\epsilon=0.3$ mm), so that free machining is achieved, which is useful for the machining temperature because it can be measured on a perpendicular surface.

In a thermal imaging measurement, the thermal camera creates an image based on the temperature difference, so the hottest element in a thermal image is white and the coldest element is black, with everything in between being placed on a shade of grey, as illustrated in Fig. 4. However, the determination of the temperature difference is not based on the actual temperature measurement, but on measuring the effect of the radiated heat, performing the mathematical calculations associated with the calibration procedure and then reporting a temperature value.

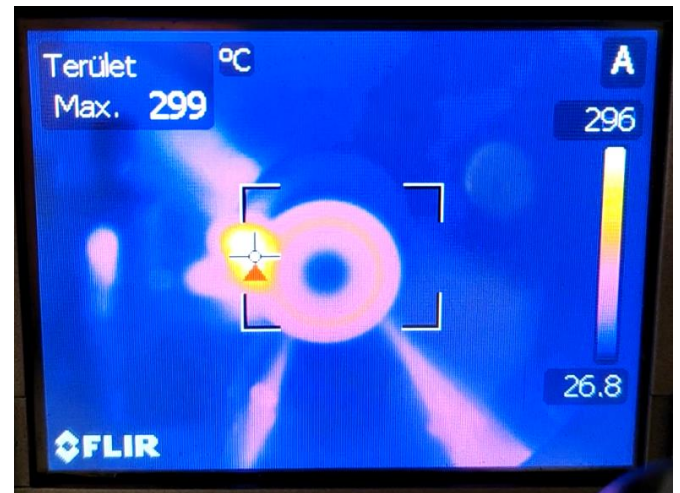


Fig. 4. Cutting temperature measurement during one test machining

The objects to be measured in real life are usually not black bodies, so their emission coefficient will be between 0.1 and 1, so the total radiation reaching the infrared camera may be a combination of emitted, transmitted and reflected radiation, which will affect the accuracy of the measurement. Since this value is different for each surface, it is advisable to achieve thermal homogeneity, so that the emission factor only needs to be well adjusted for one surface.

In order to achieve the same thermal homogeneity during the temperature measurement, and thus an accurate temperature measurement, graphite spray was applied on both the workpieces and the inserts as illustrated in Fig. 5.

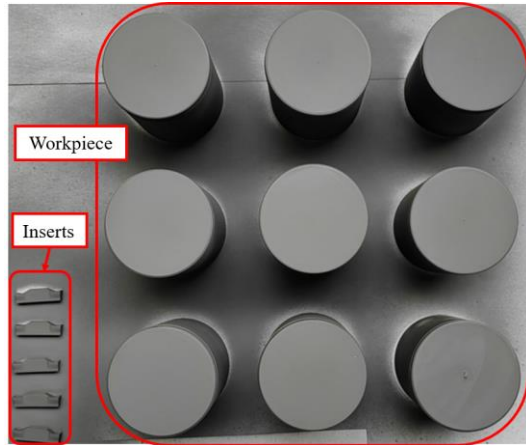


Fig. 5. The prepared workpieces and inserts for the experiment

This is important because the emissivity of both the insert and the workpiece surface is different, which would affect the measurement result. By using the graphite spray, the emissivity of the insert and the workpiece will be the same. The accuracy of the thermal imaging camera (FLIR T366) was verified using a VOLT CRAFT DETIR type tactile thermometer, which showed that the thermal imaging camera measures +10 °C more than the actual temperature. This was deduced from the subsequent results. The idea for the basis of the measurement came from the work of Dömötör et. al. (Dömötör, 2013), but the thermal homogeneity in their work was difficult to ensure due to the hybrid material pairing.

2.2. Material

The experimental material utilized in this study was austenite stainless steel categorized under the material grade X2CrNi19-11 (1.4306), the microstructure of which is illustrated in Fig. 6 and the detailed information regarding the chemical composition is provided in Table 2. The chemical composition was measured by a FOUNDRY-MASTER PRO type spectrometer in 6.0 pure argon gas to ensure precise result. Additionally, the visual documentation of the microstructure was acquired through imaging with a Zeiss STEREO Discovery V8 optical microscope.

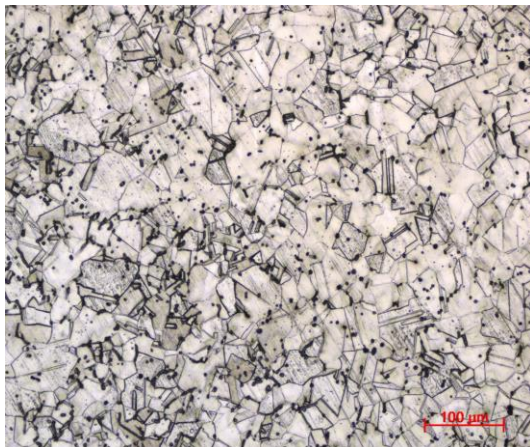


Fig. 6. Microstructure of X2CrNi19-11

Table 2. The chemical composition of X2CrNi19-11

Fe	C	Si	Mn	Cr	Ni	Co	Cu
71.2	0.03	0.12	1.38	17.9	8.00	0.11	0.48

2.3. Design of experiment

The machining parameters used during the experiments are the conventional parameters recommended by the tool manufacturer. Taguchi's method has the capability to decrease the quantity of experiments by narrowing the extensive set of input parameters and their analysed levels to give necessary and evaluable data, therefore this method was applied under the design of the experiment (Freddi, 2019; Nalbant et al., 2007). The determined two cutting parameters and their three levels are shown in Table 2. and the experimental trials were carried out using Taguchi-method. The generated 3² (L9) DoE matrix is shown in Table 3. Each machining operation was carried out under dry conditions, due to the measurement of the cutting temperature. The workpiece had a diameter of 50 mm, which was then machined to 30 mm. The insertion width was 3 mm.

Table 2. The input parameters and their levels

Input parameters	Levels		
Cutting speed, v_c (m/min)	60	80	100
Feed rate, f (mm/rev.)	0.05	0.1	0.15

Table 3. Experimental trials

E. No.	v_c (m/min)	f (mm/rev.)
1.	60	0.05
2.	60	0.1
3.	60	0.15
4.	80	0.05
5.	80	0.1
6.	80	0.15
7.	100	0.05
8.	100	0.1
9.	100	0.15

3. Results

3.1. Cutting force

The relationship between the cutting force (F) and the feed rate (f) is depicted in Fig. 7 for each cutting speed (v_c). Additionally, Fig. 8 illustrates the correlation between the cutting force and cutting speed for each feed rate. As it can be seen on the figures, the cutting force increases with an increase in the feed rate. For all three cutting speeds, it can be stated that increasing the feed rate from 0.05 mm/rev to 0.15 mm/rev increases the cutting force by a factor of almost two. At a feed rate of 0.05 mm/rev, the cutting forces are almost identical for different cutting speeds. The cutting force is the smallest for a cutting speed of 100 m/min and the largest for 60 m/min. This also means that the optimum has not been found when it comes to cutting speed, so it can be concluded that the cutting speed, and thus productivity as well, can be further increased. The smallest cutting forces were attained when machining with a feed rate of 0.05 mm/rev.

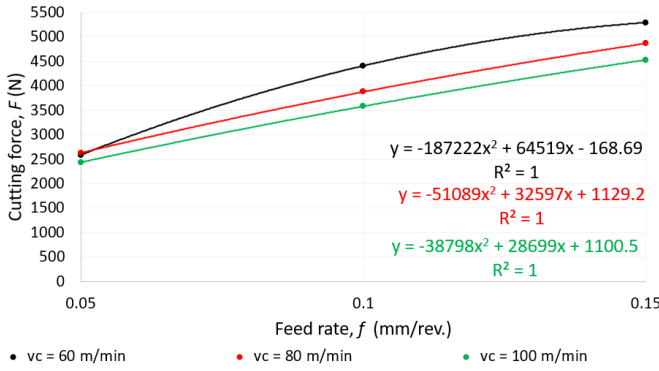


Fig. 7. Cutting force as a function of feed rate for cutting speeds of 60; 80; 100 m/min, where x representing the feed rate and y representing the cutting force

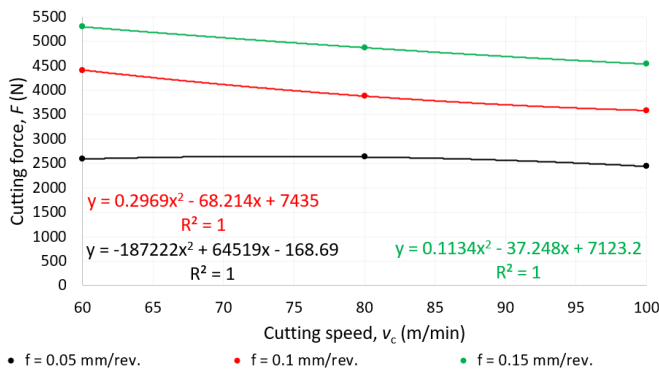


Fig. 8. Cutting force as a function of cutting speed for feed rates of 0.01; 0.1; 0.15 mm/rev, where x representing the cutting speed and y representing the cutting force

3.2. Cutting temperature

The evaluation of cutting temperature as a function of machining time in the case of 60 m/min cutting speed and 0.05 feed rate is illustrated in Fig. 9. The observed signal fluctuations can be attributed to the inherent dynamics of the turning process. To facilitate a clearer analysis of the outcomes, particular emphasis is placed on the maximum cutting temperature. In order to analyze the results more clearly, special emphasis is placed on the maximum cutting temperature. The maximum temperature data was isolated and graphed to illustrate its correlation with various cutting parameters.

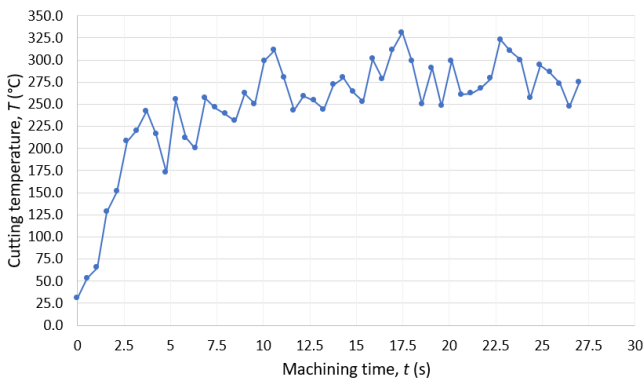


Fig. 9. Cutting temperature plotted against machining time for a cutting speed of 60 m/min and a feed rate of 0.05 mm/rev

The variation of cutting temperature (T) concerning the feed rate is presented in Fig. 10., delineating the alterations in temperature changes at different cutting speeds. Additionally, Fig. 11. depicts the relationship between cutting temperature and cutting speed for each feed rate. As the feed rate increases during machining, there is a proportional decrease in the cutting temperature. This phenomenon occurs because a larger chip cross-section is produced, thereby enhancing the heat removal from the cutting zone. However, at a specific cutting speed of 60 m/min coupled with a feed rate of 0.1 mm/rev, an abrupt and notable decrease in cutting temperature is observed, deviating from the anticipated trend. This anomaly could potentially be attributed to measurement inaccuracies or errors in the data collection process. The maximum cutting temperature was recorded at a cutting speed of 100 m/min, marking the peak temperature observed in the study, and at the lowest measured at cutting speed of 60 m/min.

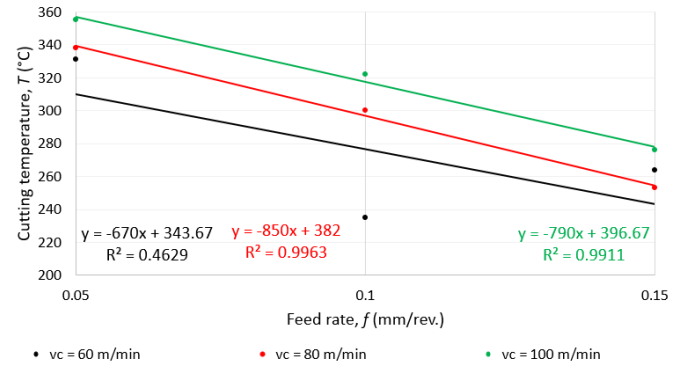


Fig. 10. Cutting temperature as a function of feed rate for cutting speeds of 60; 80; 100 m/min, where x is the feed rate and y is cutting temperature

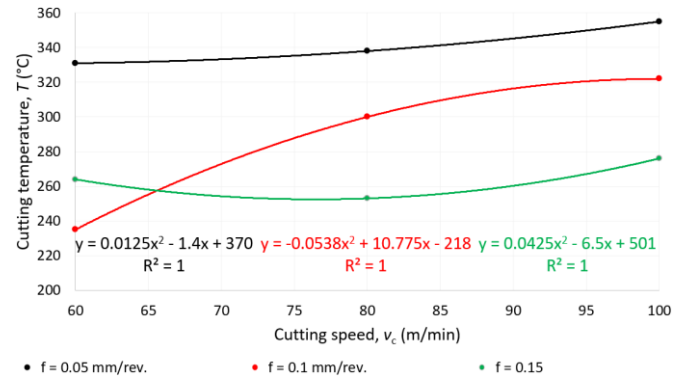


Fig. 11. Cutting temperature as a function of cutting speed for feed rates of 0.01; 0.1; 0.15 mm/rev, where x is the cutting speed and y is cutting temperature

3.3. Chip morphology

The evaluation of chip characteristics based on cutting speed and feed rate is shown in Fig. 12. Optimum chip formation was observed at a cutting speed of 80 m/min and a feed rate of 0.05 mm/rev, with the most favorable chip breaking achieved by this specific parameter setting. This configuration presents an ideal balance for efficient chip breaking and good handling. As the feed rate increases, a gradual decrease in chip

diameter can be seen. This reduction is accompanied by a reduction in chip breakage due to the larger chip cross-section, resulting in longer chips less suitable for efficient handling and disposal. As the cutting speed increases, a proportional change in chip color can be observed, especially an increase in discoloration and yellowish tint. This discoloration is consistent with the maximum recorded cutting temperature, indicating a relationship between the thermal conditions of the cutting process and chip properties. Furthermore, an interesting observation is noted concerning the effect of increased feed rates on chip shearing. As the feed rate rises, the chips undergo greater levels of shearing, likely linked to the heightened cutting force exerted during machining operations.



Fig. 12. Chip evaluation as a function of cutting speed and feed rate

4. Conclusion

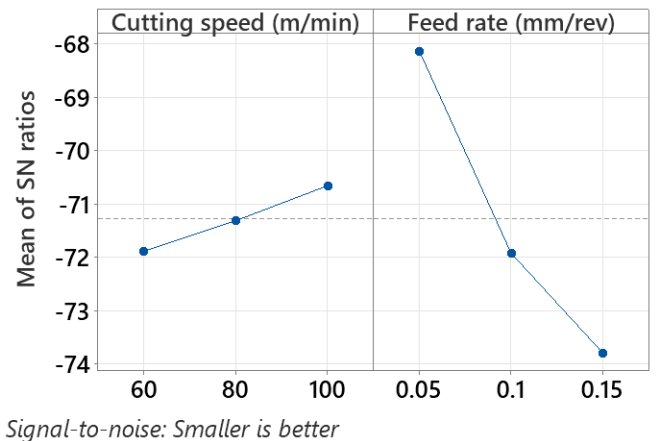
The objective of this research paper was to examine how variations in cutting speed and feed rate influence crucial parameters such as cutting forces, cutting temperature and chip evaluation. The effects of cutting speed and feed rate on cutting force are illustrated in Fig. 13 and cutting temperature in Fig. 14. The ultimate goal of this investigation was to minimize cutting forces and cutting temperature, crucial factors for efficient machining and tool failure.

To evaluate the optimal technological parameter settings, the Signal-to-noise (SN) ratio was used, utilizing the “Smaller is better” approach via Eq. (3), where Y signifies the responses for the specified combination of factor levels and n denotes the number of responses in the factor level combination. The results from these analyses consistently indicated that the feed rate exerted the most significant influence on both cutting force and cutting temperature. This finding was clearly illustrated in the diagrams, emphasizing the critical role of feed rate adjustments in controlling and optimizing cutting forces and cutting temperatures during machining processes.

$$\frac{S}{N} = -10 \cdot \log \left(\frac{\sum(1/Y^2)}{n} \right) \quad (3)$$

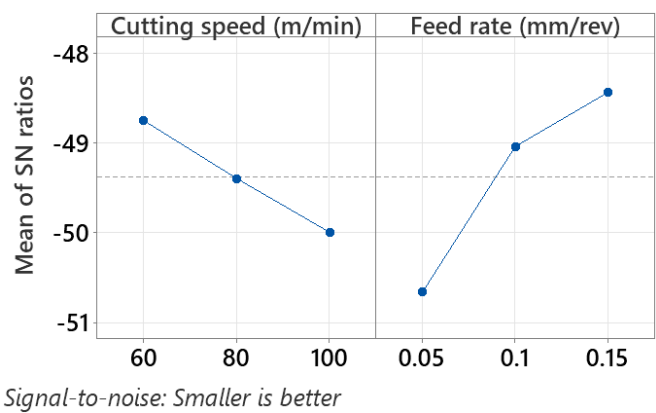
The authors state the following conclusions:

- The findings emphasize that among the cutting speed and feed rate studied, the feed rate stands out as exerting the most significant influence on crucial aspects of the machining process. This impact is notably evident in the behaviours of cutting force, cutting temperature, and chip evaluation, as explicitly depicted and detailed in Fig. 13-14.
- The biggest cutting force has been measured when machined with a 0.15 mm/rev feed rate.
- The smallest cutting force has been measured when machined with a 100 m/min cutting speed, which means that it can be increased, therefore the productivity can be increased as well.
- The chips became more compressed, discoloured and the chip breakage was worse when increasing the feed rate.
- The rate of discoloration change is often directly related to the feed rate. This phenomenon occurs because the chips generated during the machining process have a larger cross-sectional area and have the ability to absorb more heat from the cutting zone. Therefore, increased feed rate contributes to greater heat dissipation, resulting in greater discoloration of the processed material.



Signal-to-noise: Smaller is better

Fig. 13. The influence of cutting speed and feed rate on cutting force



Signal-to-noise: Smaller is better

Fig. 14. The influence of cutting speed and feed rate on cutting temperature

Reference

- Acayaba, G. M. A., de Escalona, P. M., 2015. Prediction of surface roughness in low speed turning of AISI316 austenitic stainless steel. *CIRP Journal of Manufacturing Science and Technology*, 11, 62-67, DOI: 10.1016/j.cirpj.2015.08.004.
- Bharasi, N. S., Pujar, M.G., Das, C.R., Philip, J., Thyagarajan, K., Paneerselvi, S., Moitra, A., Chandramouli, S., Karki, V., Kannan, S., 2019. Microstructure, corrosion and mechanical properties characterization of AISI type 316L(N) stainless steel and modified 9Cr-1Mo steel after 40,000 h of dynamic sodium exposure at 525 °C. *Journal of Nuclear Materials*, 516, 84-99, DOI: 10.1016/J.JNUCMAT.2019.01.012
- Buranská, E., Buranský, I., Kritikos, M., Gerulová, K., Liška, J., (2019). Cutting Environment Impact on the Aluminium Alloy Machining, *Vedeckee Prace Materialovotechnologickej Fakulty Slovenskej Technickej Univerzity V Bratislave So Sídrom V Trnave*. 27(44), 21-28, DOI: 10.2478/rput-2019-0002
- Dömötör, F., Vehovszky, B., Weltsch, Z., Németh, Sz., Terpó, Gy., 2013. Complex Process Monitoring of Cutting Hybrid Metal Structures. *Periodica Polytechnica Transportation Engineering*, 41(2), 87-94, DOI: 10.3311/PPtr.7107
- Ezugwu, E.O., Wang, Z.M., 1997. Titanium alloys and their machinability—a review. *Journal of Materials Processing Technology*, 68(3), 262-274, DOI: 10.1016/S0924-0136(96)00030-1
- Freddi, A., Salmon, M., 2019. Introduction to the Taguchi Method, *Design Principles and Methodologies*. Springer Tracts in Mechanical Engineering, Springer, Cham.
- Gerth, J., Gustavsson, F., Collin, M., Andersson, G., Nordh, L.-G., Heinrichs, J., Wiklund, U., 2014. Adhesion phenomena in the secondary shear zone in turning of austenitic stainless steel and carbon steel. *Journal of Materials Processing Technology*, 214(8), 1467-1481, DOI: 10.1016/J.JMATPROTEC.2014.01.017
- Gökkaya, H., Nalbant, M., 2007. The effects of cutting tool geometry and processing parameters on the surface roughness of AISI 1030 steel. *Materials & Design*, 28(2), 717-721, DOI: 10.1016/j.matdes.2005.09.013
- Kónya, G., Kovács, Z. F., 2023. The Comparison of Effects of Liquid Carbon Dioxide and Conventional Flood Cooling on the Machining Conditions During Milling of Nickel-based Superalloys. *Periodica Polytechnica Mechanical Engineering*, DOI: 10.3311/PPme.22265
- Kónya, G., Kovács, Zs. F., Kókai, E., 2022. Milling of Nickel-based superalloy by Trochoidal Strategies, 2022 IEEE 22nd International Symposium on Computational Intelligence and Informatics and 8th IEEE International Conference on Recent Achievements in Mechatronics. *Automation, Computer Science and Robotics (CINTI-MACRo)*, Targu-Mures, Romania, 1-6.
- Kovács, Z. F., Viharos, Z. J., Kodácsy, J., 2022. Improvements of surface tribological properties by magnetic assisted ball burnishing. *Surface and Coatings Technology*, 437, 128317, DOI: 10.1016/j.surfcoat.2022.128317
- Królczyk, G. M., Nieslony, P., Legutko, S., 2015. Determination of tool life and research wear during duplex stainless steel turning. *Archives of Civil and Mechanical Engineering*, 15(2), 347-354, DOI: 10.1016/J.ACME.2014.05.001/METRICS
- Kulkarni, A. P., Joshi, G. G., Karekar, A., Sargade, V. G., 2014. Investigation on cutting temperature and cutting force in turning AISI 304 austenitic stainless steel using AlTiCrN coated carbide insert. *International Journal of Machining and Machinability of Materials*, 15(3-4), 147-156, DOI: 10.1504/IJMMM.2014.060546
- Kun, K., Kodácsy, J., Vaczó, D., Kovács, Zs. F., 2019. Machinability of Ni-based Superalloys by Indexable End Mills. *Acta Materialia Transylvanica*, 2(1), 49-54, DOI: 10.33924/amt-2019-01-08
- Leksycki K., Maruda, R. W., Feldshtein, E., Wojciechowski, S., Habrat, W., Gupta, M. K., Królczyk, G. M., 2023. Evaluation of tribological interactions and machinability of Ti6Al4V alloy during finish turning under different cooling conditions. *Tribology International*, 189, 109002, DOI: 10.1016/j.triboint.2023.109002
- Móricz, L., Viharos, Z. J., 2022. Investigation of ductile/brittle chip formation zone in the context of manufactured geometry with different CAM paths strategies. *IFAC-PapersOnLine*, 55(10), 2300-2305, DOI: 10.1016/j.ifacol.2022.10.051
- Nalbant, M., Gökkaya, H., Sur, G., 2007. Application of Taguchi method in the optimization of cutting parameters for surface roughness in turning. *Materials & Design*, 28(4), 1379-1385, DOI: 10.1016/j.matdes.2006.01.008.
- Saketi, S., Östby, J., Olsson, M., 2016. Influence of tool surface topography on the material transfer tendency and tool wear in the turning of 316L stainless steel. *Wear*, 368-369, 239-252, DOI: 10.1016/j.wear.2016.09.023
- Smith, G. T., 1989. *Advanced Machining – The Handbook of Cutting Technology*. IFS Pub/Springer Verlag, Germany.
- Radek, N., 2023. Properties of WC-Co coatings with Al2O3 addition. *Production Engineering Archives*, 29(1), 94-100, DOI: 10.30657/pea.2023.29.11
- Sipos, S., 2018. A new method for analysing the efficiency of cutting inserts. *IOP Conference Series: Materials Science and Engineering*, 448(1), 012043, DOI: 10.1088/1757-899X/448/1/012043
- Sonawane, S., Wangikar, S., Pukale, K., 2021. Multi-Independent Optimization while Turning of Inconel-600 alloy using Grey Interactive Exploration. *Production Engineering Archives*, 27(4), 277-282, DOI: 10.30657/pea.2021.27.37
- Szczotkarz, N., Mrugalski, R., Maruda, R. W., Królczyk, G. M., Legutko, S., Leksycki, K., Dębowski, D., Pruncu, C. I., 2021. Cutting tool wear in turning 316L stainless steel in the conditions of minimized lubrication. *Tribology International*, 156, 106813, DOI: 10.1016/j.triboint.2020.106813
- TaeguTec cutting tool catalogue, [online] Available at: <https://www.imc-companies.com/TaeguTec/ttkCatalog/item.aspx?cat=6110853&fnum=623&mapp=TG&app=0&GFSTYP=M&isoD=1>, [Accessed at: 01. 07. 2023.] a.
- TaeguTec cutting tool catalogue, b[online] Available at: <https://www.imc-companies.com/taegutec/ttkCatalog/item.aspx?cat=2801655&fnum=649&mapp=TG&app=51&GFSTYP=M&isoD=1>, [Accessed at: 01. 07. 2023.] b.
- Tschätsch, H., Reichelt, A., 2009. *Tool life T.*, Applied Machining Technology, Springer, Berlin, Germany.
- Venkatesan, K., (2017). The study on force, surface integrity, tool life and chip on laser assisted machining of inconel 718 using Nd:YAG laser source. *Journal of Advanced Research*, 8(4), 407-423, DOI: 10.1016/j.jare.2017.05.004